RSC Advances

PAPER

View Article Online
View Journal | View Issue

Cite this: *RSC Adv.*, 2026, **16**, 19437

Tolerances in microfluidic master molds: a comparison of 3D printing and micromilling

Daniel Chavarria, *[a] Immanuel Ojetola,[b] Maria L. Russotti,[c] Alexis K. Yates[afg] and Ethan S. Lippmann *[acdefg]

3D printing and micromilling are increasingly becoming more accessible alternatives to cleanroom photolithography for the fabrication of master molds that can be subsequently used for cast patterning soft material microfluidic devices. However, there is a lack of characterization on the fabrication tolerances of 3D printed and micromilled master molds, which can influence microdevice performance. In this work, we present an in-depth characterization of master molds fabricated using 3D printing *versus* micromilling. We utilized profilometry to examine the accuracy of fabricated channel dimensions and assess surface finish. We then proceed to assess differences in performance between devices cast from 3D printed or micromilled master molds by creating microfluidic splitting devices or flow focusing devices. We then evaluated their performance in a low-flow rate splitting application and in the generation of gelatin microspheres respectively. For both applications micromilling resulted in a significantly smoother surface finish when compared to 3D printed master molds. On average, both fabrication modalities fell short in accurately fabricating channel dimensions (~50 μm) when compared to the original CAD model of the microfluidic master mold. In our low-flow rate application, there were no significant differences in flow rate splitting efficiency between microfluidic devices cast from either 3D printed or micromilled master molds. In our assay for generating gelatin microspheres, the smoother surface finish of the CNC master molds resulted in a flow focusing devices that generated significantly larger gelatin microspheres. Overall, this investigation serves as a useful guide for future investigators on the fabrication tolerances of soft material microfluidic devices cast from 3D printed and micromilled master molds.

Received 2nd February 2026
Accepted 7th April 2026

DOI: 10.1039/d6ra00916f

rsc.li/rsc-advances

Introduction

Microfluidics fabrication techniques have greatly advanced during the past three decades. Photolithography initially emerged as one of the first fabrication techniques for creating silicon microfluidic devices for chemical analysis such as that of Reston and Koselar who created a miniature gas chromatography system.[1] With the emergence of better photoresist materials, such as SU-8, the first microfluidic master molds were developed which could be used for soft lithography.[2] Soft lithography relies on a master mold that contains a negative of the intended device design, whereby casting a positive using soft materials such as polydimethylsiloxane (PDMS) creates the patterned microdevice. Soft lithography is a cost-effective method for pattern transfer and the fabrication of microfluidic devices, and for much of its history, creation of master molds for soft lithography remained restricted to specialized cleanrooms which limited rate of adoption. New fabrication technologies such as 3D printing and micromilling have emerged as alternatives to the use of photoresist materials for the fabrication of microfluidic master molds. 3D printing has gained wide popularity due to cost-effectiveness and accessibility of commercially available 3D printers, which are generally capable of creating micron-size features.[3–5] On the other hand, micromilling is more cost-prohibitive relative to 3D printing but also potentially more favorable than photopatterning approaches due to cost and accessibility associated with cleanrooms. Micromilling offers select advantages over 3D printing in terms of the number of materials that can be used for subtractive fabrication of master molds, including a variety of polymers,[6] metals,[7–9] and ceramics[10] that can be used to create micron-size features. However, there is a lack of characterization of how 3D printing *versus* micromilling influences master mold features. As such, in this study, we characterize the surface finish

---

[a] Department of Chemical and Biomolecular Engineering, Vanderbilt University, Nashville, TN, USA. E-mail: daniel.chavarria@vanderbilt.edu; ethan.s.lippmann@vanderbilt.edu
[b] School for Science and Math at Vanderbilt, Vanderbilt University, Nashville, TN, USA
[c] Department of Biomedical Engineering, Vanderbilt University, Nashville, TN, USA
[d] Vanderbilt Brain Institute, Vanderbilt University, Nashville, TN, USA
[e] Department of Neurology, Vanderbilt University Medical Center, Nashville, TN, USA
[f] Interdisciplinary Materials Science Program, Vanderbilt University, Nashville, TN, USA
[g] Vanderbilt Memory and Alzheimer's Center, Vanderbilt University Medical Center, Nashville, TN, USA

and tolerances of both 3D printed and micromilled master molds to assess their reproducibility and accuracy. We also explored various feed rate velocities for micromilling to assess differences in tolerances and surface finish in aluminum master molds. Experimental results revealed that both 3D printing and micromilling resulted in comparable master molds with similar tolerances and surface finish irrespective of feed rate for the micromilled master molds. Overall, our study serves as a useful guide for user expectations when fabricating master molds using 3D printing and micromilling.

Materials and methods

Fabrication of master molds

The μ-split chip was designed in CAD software (Fusion 360; Autodesk) as previously described.[11] The master molds for the μ-split chips were fabricated using a 3D printer (Form 3; Formlabs) or CNC mill (Haas 1 CM-1). 3D printed master molds were printed using black resin (Black V4.1; Formlabs). The master molds were then thoroughly washed to remove excess resin, dried overnight, and cured with the Formlabs cure chamber for 30 min at 60 °C. The 3D printed master molds were then coated with parylene-C dimer as previously described.[4] For micromilled master molds, aluminum stock (9146T69; McMaster-Carr) was milled on the CNC mill using 0.25″, 0.125″, and 0.06″ square end mills (8918A51, 8918A41, 8916A66; McMaster-Carr). Additional information regarding CAD files, generated tool paths, feeds and speeds are available at GitHub.

Fabrication of microfluidic splitter devices

To create μ-split devices, PDMS (Sylgard 182; Dow Corning) elastomer and curing agent were mixed at a 9 : 1 ratio and poured onto the 3D printed or micromilled master molds. The master molds were then placed in a vacuum chamber to remove all bubbles and subsequently heat-cured at 50 °C for 2 hours or overnight. After heat-curing, the solidified PDMS was carefully removed from the master molds, and a biopsy punch (1.5 mm) was used to create inlets and outlets for the channels. Debris was removed from the surface of the PDMS using tape and the μ-split devices were plasma bonded to a precleaned microscope glass slide (CLS294875X25; Sigma-Aldrich).

Peristaltic pump perfusion system

A custom-made peristaltic pump perfusion system was designed using CAD software (Fusion 360; Autodesk). The electronic controller for the peristaltic pump was modified from a previous publication.[12] Briefly, the microfluidic electronic controller system utilizes a single-board computer (3A+; Raspberry Pi), a breakout board (HD040; Xiken Electronic Technology Co., Ltd), touchscreen display (SC1227; Raspberry Pi), motor driver board (112779; SparkFun Electronics), and a stepper motor (5-17HS19-2004S1; StepperOnline) with a 12v power supply (ALT-1205; ALITOVE). The software for the peristaltic pump device was developed in-house utilizing a programming language (Python; Python Software Foundation). The software was modified from a prior microdevice design used to control a spinning bioreactor.[13]

Volumetric flow rate measurements using microfluidic device splitters

To assess the volumetric flow rate profiles of each μ-split device, we utilized two liquid flow sensors (SLI-2000, SLI-0430; Sensirion) directly attached to each of the splitter outlets in turn with an equal length tubing attached to the outlet that did not have the sensor. Measurements were averaged over the duration of the testing period, lasting approximately 30 seconds each.

Measuring tolerances of master molds using stylus profilometer

Tolerances of the 3D printed and micromilled master molds were measured using a stylus profilometer (Bruker Dektak 150) using a 12.5 μm diamond tip set at 12 mg of force. The length of scan of the stylus profilometer was set to 2000 μm with a resolution of 0.067 μm per sample. Surface roughness was measured at the inlet and both outlets of the microfluidic splitter device. Three measurements were completed per sample. All measurements were performed at the Vanderbilt Institute of Nanoscale Science and Engineering (VINSE).

Calculation of flow rate splitting efficiency

To assess the efficiency by which our μ-split device evenly split flow, we utilized the following formula:

$$Q_{\mathrm{SE}} = Q_{\mathrm{O1}}/Q_{\mathrm{O2}}$$

Here Q_{SE} represents flow rate splitting efficiency, Q_{O1} represents the flow rate at the first outlet, and Q_{O2} represents the flow rate at the second outlet. A flow rate splitting efficiency ratio of 1 indicates the device equally splits the flow rate between both outlets.

Statistical analysis

All statistical analysis were performed using statistical analysis software (Prism; GraphPad). All experimental results are shown as mean ± standard error of the mean (SEM). Multiple comparisons between groups were analyzed by one-way ANOVA followed by Tukey's post hoc test. A two-tailed probability value $p < 0.05$ was considered statistically significant. An independent replicate for each experiment was considered as a singular master mold or μ-split chip.

Generation of gelatin microspheres using flow focusing microfluidic device

The microspheres in this study were composed of 5% porcine gelatin (G1890; Sigma-Aldrich) dissolved in ultrapure water (10977–015; invitrogen). The gelatin solution was heated to 37 °C then sterile filtered through a 22 μm syringe filter (SLMP025SS; Millitex). The oil solution was composed of 2% Span 80 (S6760; Sigma-Aldrich) in light mineral oil (330779; Sigma-Aldrich). The oil and gelatin solutions were pumped into the microfluidic chip by syringe pumps (Pump 11 Elite Infusion/Withdrawal Programmable Single Syringe; Harvard Apparatus) and connected *via* PTFE tubing (50929; Hach Company). The flow rate of the oil phase was set to 400 µl min^{-1}, and the flow rate of the gelatin solution was set to 40 µl min^{-1}. During microsphere formation, the microfluidic chip was placed on a hot plate at 37 ° C and the collection plate was placed on top of ice to facilitate thermal crosslinking of the gelatin.

Results

Fabrication of microfluidic splitter master molds using 3D printing and micromilling

To examine the tolerance differences of 3D printed and micromilled master molds, we utilized a microfluidic splitter device design by our lab that we refer to as µ-split, which was developed in our lab to facilitate even fluid splitting under low-flow applications.[11] Briefly, the microfluidic splitter device consists of one inlet channel that splits into two outlet channels using a wishbone geometry (Fig. 1A and B). The inlet channel of the µ-split device was designed to be 600 µm wide by 300 µm tall (Fig. 1C) while the two outlet channels of the µ-split device were designed to be 300 µm wide by 300 µm tall each (Fig. 1D). To 3D print the master mold of the µ-split device, we utilized an SLA 3D printer and then parylene coated the printed mold to create an inert surface as described in our prior work.[4] Triplicates of the 3D-printed and parylene coated µ-split device were generated for experimentation (Fig. 2). For the micromilled µ-split master molds, we used aluminum blanks and a compact CNC mill. We first utilized a 0.25″ flat end mill to flatten out the stock. Then we proceeded to utilize 0.125″ flat end mill to carve out the geometry of the µ-split device. In these experiments, we

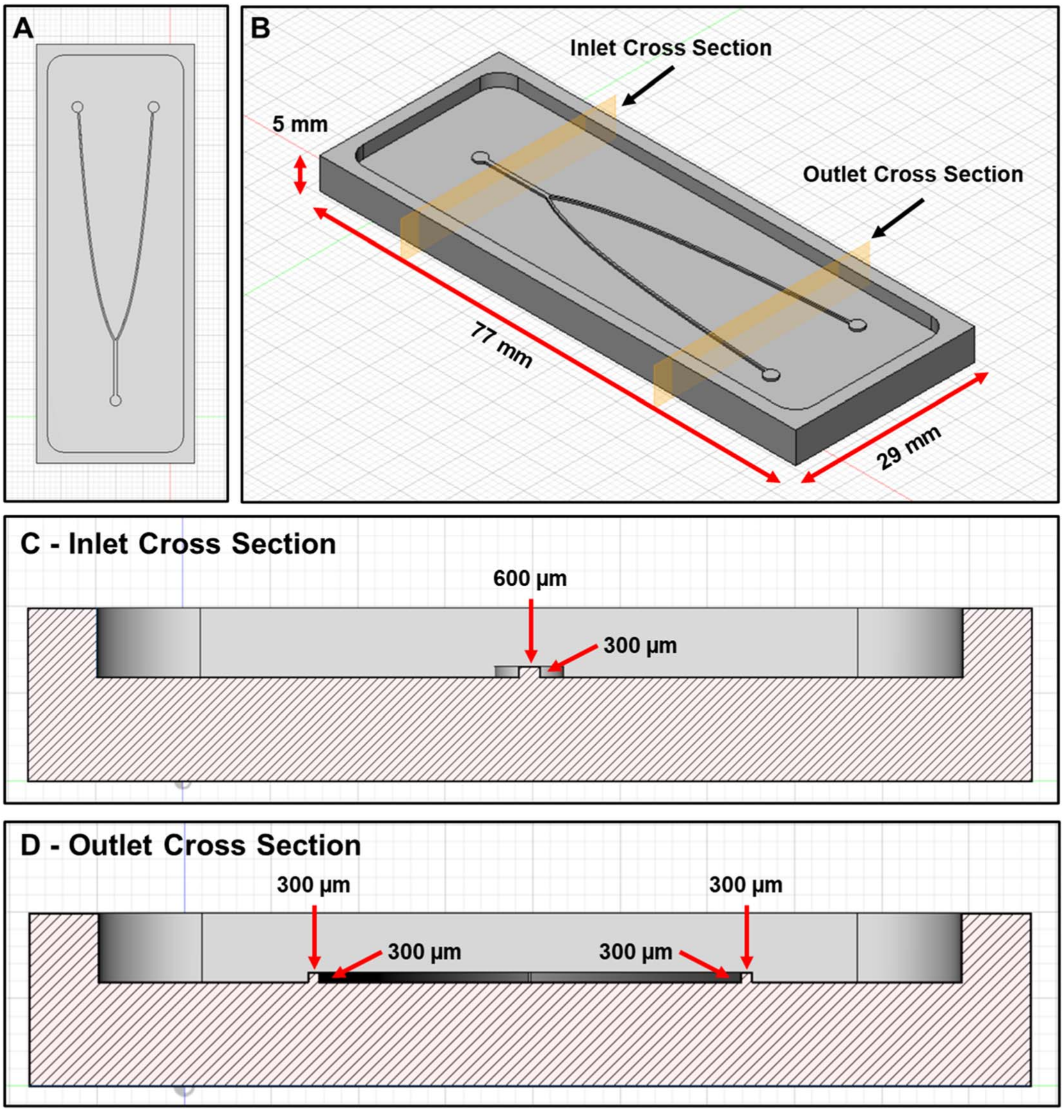

Fig. 1 Diagrams of microfluidic splitter master mold. Diagrams generated utilizing computer-aided design software of (A) top and (B) angled view of master mold for casting a microfluidic splitter device. Diagrams of (C) inlet and (D) outlet cross section of master mold for casting a microfluidic splitter device.

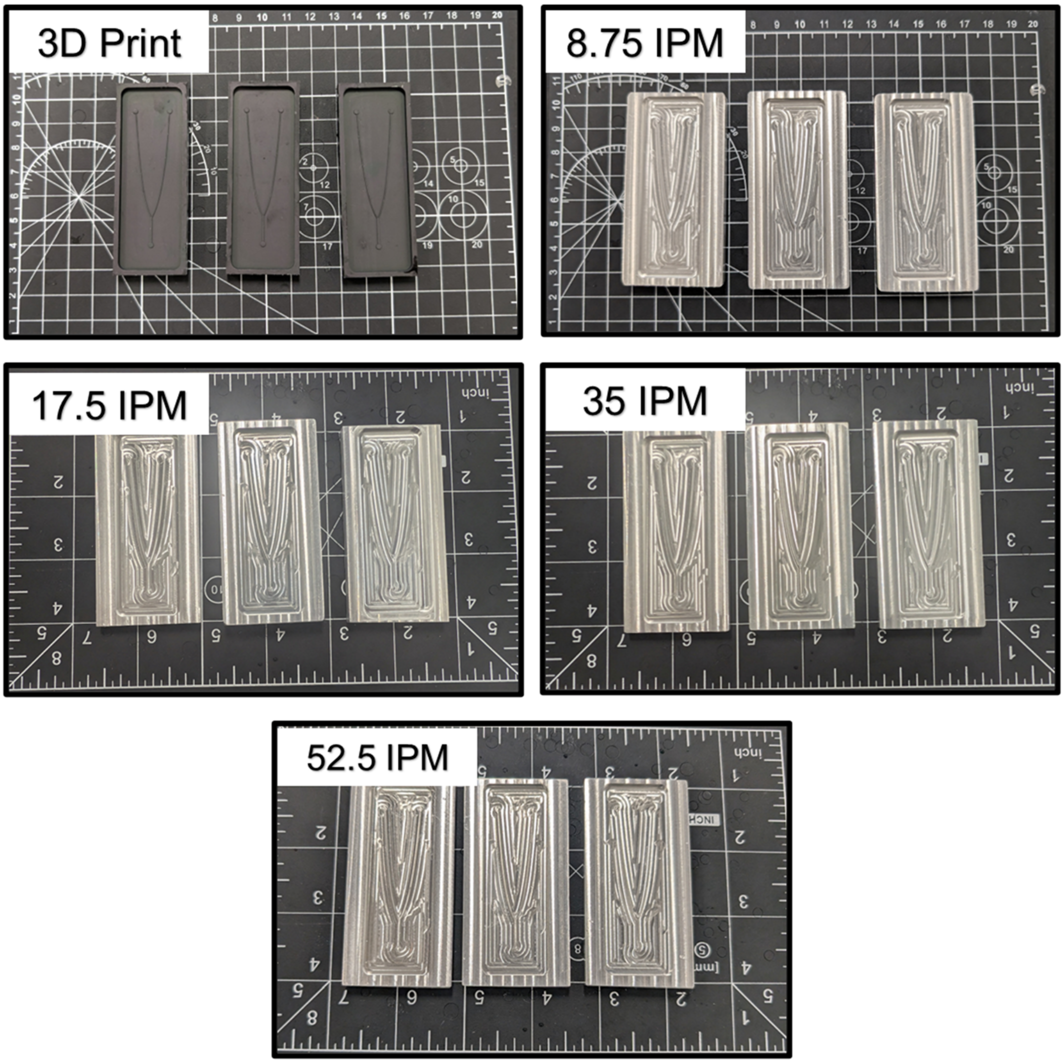

Fig. 2 Pictures of 3D printed and CNC machined microfluidic splitter master molds. Top view pictures of 3D printed, and micromilled microfluidic splitter master molds fabricated using a form 3 SLA printer and Haas CM-1 compact mill correspondingly. Micromilled master molds were fabricated using increasing feeding rates (8.75, 17.5, 35, and 52.5 inches per minutes [IPM]) using a titanium coated 1/8″ high speed steel flat end mill.

varied the feed rate of the 0.125″ flat end mill while maintaining the same spindle rotational speed. This allowed us to study differences in the surface finish created by varying the CNC mill feed rate. Throughout the course of experimentation, we generated triplicates of the μ-split devices milled at 8.75, 17.5, 35, and 52.5 inches per minute (IPM; Fig. 2). We also attempted to mill versions of the μ-split device using feed rates of 70 and 140 IPM. However, at these feed rates the 0.125″ flat end mill broke before finishing. Finally, we utilized a 0.06″ flat end mill to mill the bifurcation junction of μ-split device where the inlet channels split into the two outlet channels, given the finer features of this section.

Characterization of fabricated master mold tolerances using profilometry

To assess differences in fabrication tolerances, we utilized a stylus profilometer to measure the surface finish of the 3D printed and micromilled μ-split master molds. We recorded profilometer measurements at an intermediary point of the inlet channel and both outlet channels of each fabricated master mold. Based on the CAD drawing for the μ-split master mold, the inlet channel cross section of the μ-split device would result in a rectangle measuring 600 μm wide by 300 μm tall (Fig. 3A). We plotted the inlet channel profilometer measurements for each fabricated μ-split master mold and noticed all fabrication modalities (3D printed or micromilled) resulted in a trapezoidal geometry for the cross section of the inlet channels (Fig. 3B–F). All fabrication modalities resulted in a wider inlet channel (∼700 μm) with no statistically significant difference between any of the μ-split master molds fabricated using 3D printing or micromilling (Fig. 4A). The average height of the inlet channel for the 3D printed and micromilled master molds milled at 17.5, 35, and 52.5 IPM were shorter (∼250 μm) than the CAD model (300 μm; Fig. 4B). The master mold milled at

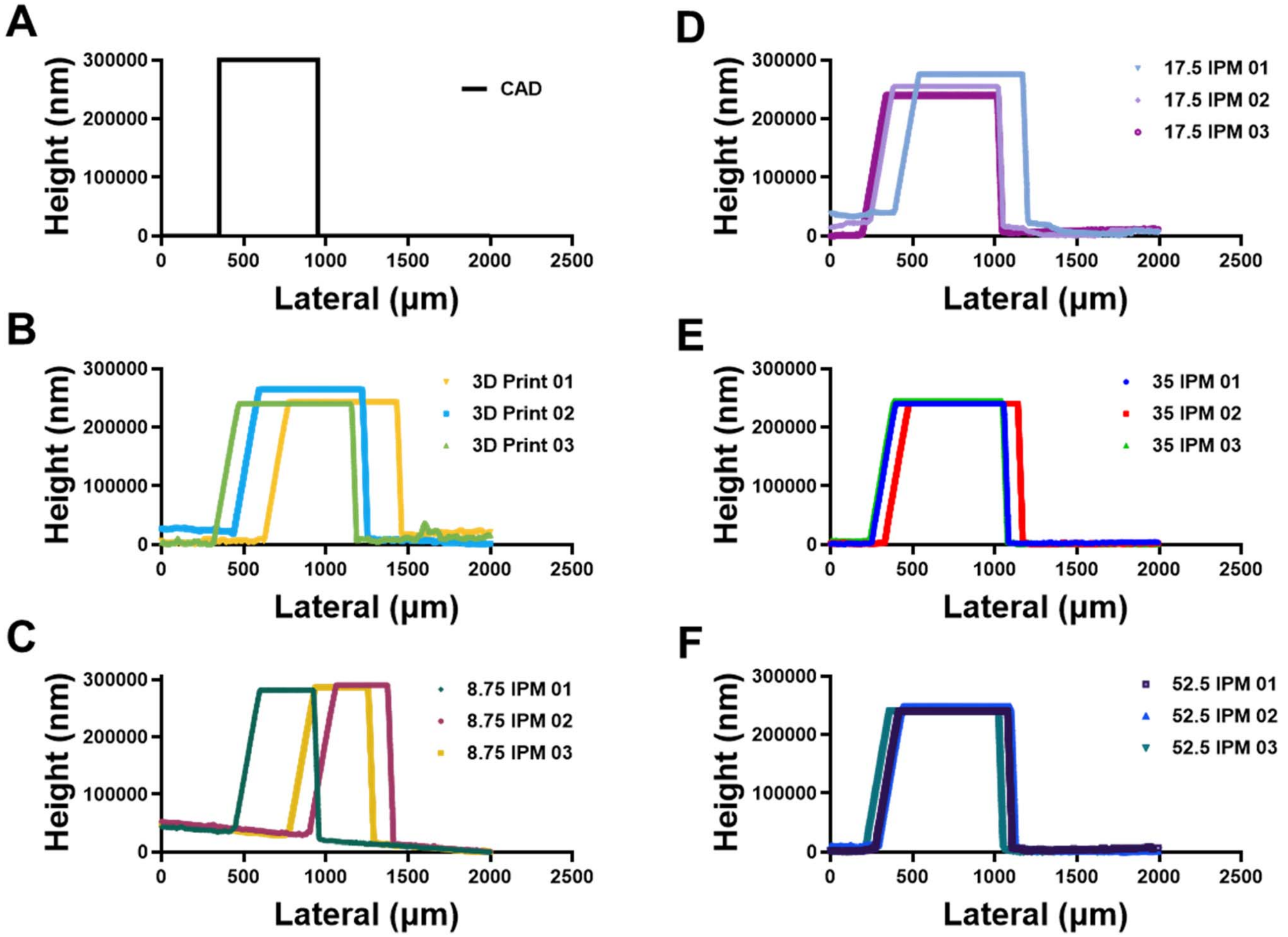

Fig. 3 Inlet profilometer measurements of master molds of microfluidic splitters. (A) Graph of theoretical inlet profilometer measurements of microfluidic splitter master mold retrieved from CAD file. Profilometer measurement from microfluidic splitter inlet master molds fabricated using (B) 3D printing and (C–F) micromilling. Data represents profilometer measurements from $N = 3$ from single master molds per fabrication method.

8.75 IPM yielded an average inlet channel height (301 µm) that was very close to the CAD model, resulting in a statistically significant difference compared to the rest of the 3D printed and micromilled master molds using different feed rates (Fig. 4B). Although the width and height of the inlet channels for the 3D printed master molds and master molds micromilled at 17.5, 35, and 52.5 IPM deviated from the CAD model, the average cross sectional area for these master molds (~181 000 µm^2; Fig. 4C) closely approximated the cross sectional area of the inlet channel in the CAD model (180 000 µm^2). The average cross-sectional area for the inlet channels of the µ-split master molds milled at 8.75 IPM was larger (211 235 µm^2) and significantly different from the rest of the fabricated master molds (Fig. 4C).

We repeated the same profilometry analysis for the outlet channels of all the fabricated µ-split master molds. The outlet channel from the CAD model were designed to have a rectangular cross-sectional geometry measuring 300 µm wide and 300 µm tall (Fig. 5A). When we plotted the profilometry measurements from all outlet channels of the 3D printed and micromilled master molds, we noticed the same trapezoidal geometry in all the outlet channels as seen in the inlet channels (Fig. 5B–F). The average width for all micromilled master molds was wider than the CAD model (300 µm) ranging from 426 to 444 µm (Fig. 6A). The 3D printed µ-split master molds had even wider channels (506 µm) when compared to the micromilled master molds, which resulted in a statistically significant difference (Fig. 6A). The profilometer measurements also revealed no differences in height of the outlet channels fabricated using 3D printing and micromilling (17.5, 35, 52.5 IPM), resulting in average shorter channels (242–260 µm) when compared to the CAD model (300 µm; Fig. 6B). The master mold micromilled at 8.75 IPM more closely approximated the CAD model height, averaging an outlet channel height of 288 µm, which was significant different from the rest of the 3D printed and micromilled master molds (Fig. 6B). All fabrication modalities resulted in wider average cross-sectional area when compared to the CAD model (90 000 µm^2; Fig. 6C). The average cross-sectional area between µ-split master molds micromilled at 8.75 IPM (122 039 µm^2) was significantly different from the

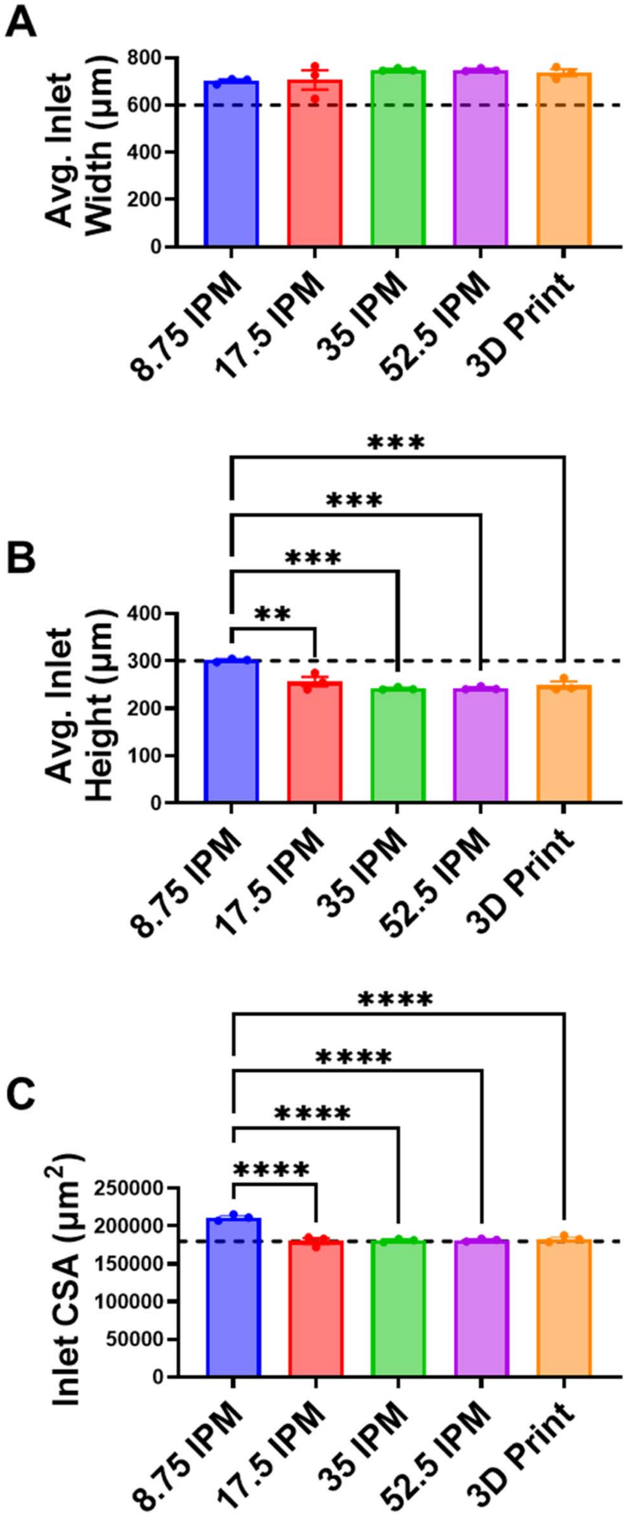

Fig. 4 Quantification of inlet profilometer measurements. Inlet profilometer measurement plots from each master mold were used to measure the average inlet (A) width, (B) height and (C) cross-sectional area (CSA). Data represents mean ± SEM from $N = 3$ from single master mold inlet per fabrication method. Statistical significance was calculated using a one-way ANOVA comparing all the fabrication modalities to each other (8.75 IPM *vs.* 17.5 IPM, 8.75 IPM, *vs.* 35 IPM, 8.75 IPM *vs.* 52.5 IPM, 8.75 IPM *vs.* 3D print, 17.5 IPM *vs.* 35 IPM, 17.5 IPM *vs.* 52.5 IPM, 17.5 IPM *vs.* 3D print, 35 IPM *vs.* 52.5 IPM, 35 IPM *vs.* 3D print, and 52.5 IPM *vs.* 3D print; **, $p < 0.01$; ***, $p < 0.001$; ****, $p < 0.0001$). Dotted lines represent the width, height, and cross-sectional area from the CAD model of the µ-split master mold.

master molds micromilled at 35 IPM (105 220 µm^2; Fig. 6C). There were also significant differences between the average cross-sectional area of the 3D printed master molds (131 950 µm^2) compared to the master molds micromilled at 17.5, 35, and 52.5 IPM (108 275, 105 220, and 108 231 µm^2, respectively; Fig. 6C). Lastly, we characterize the surface finish of µ-split device by obtaining profilometry measurements at three random flat segments excluding the inlet or outlet channels from of each master mold. We then calculated the surface roughness by subtracting the lowest profilometry measurement from the highest profilometry measurement. Overall, the micromilled master molds had a smooth surface finish with the average surface roughness ranging from 362 to 388 nm (SI Fig. 1). The 3D printed master molds had a significantly higher average surface roughness (1772 nm) compared to the micromilled master molds (SI Fig. 1).

Effects of microfluidic fabrication tolerances on low-flow rate splitting

This µ-split device is ideal for testing the effects of fabrication tolerances on low-flow rate conditions, as microfluidic splitting at low-flow rates is highly sensitive to small aberrations in surface finish that alter the channel dimensions as we have previously demonstrated. To test how differences in microfluidic tolerances might affect low-flow rate splitting, we cast PDMS devices using each of the fabricated µ-split master molds. The PDMS devices were then connected to a custom peristaltic pump (SI Fig. 1A) to generate flow (SI Fig. 1B). We tested various inlet flow rates including 5, 19, 35, 55, and 100 µl min^{-1} while collecting volumetric measurements at each outlet (Fig. 7A).

The lowest inlet flow rate setting of 5 µl min^{-1} resulted in the most irregular low-flow splitting at the outlets of all the PDMS devices cast from the micromilled master molds, yielding either stalled flow or back flow at the outlets (Fig. 7B). The PDMS devices cast from the 3D printed master molds resulted in an average flow rate of 1.83 µl min^{-1} (Fig. 7B). At a flow rate of 19 µl min^{-1}, only the PDMS devices cast from the master molds micromilled at 17.5 and 52.5 IPM had any backflow (Fig. 7C). The PDMS µ-split devices from the master molds micromilled at 17.5 and 35 IPM had outlet flow rates averaging 2.27 and 5.20 µl min^{-1} (Fig. 7C). The rest of the PDMS µ-split devices (8.75 IPM, 52.5 IPM, and 3D print) had stalled flow at the outlets (Fig. 7C). An inlet flow rate of 35 µl min^{-1} resulted in an average positive flow rate for all the PDMS µ-split devices although the PDMS µ-split devices cast from the master molds micromilled at 17.5 and 35 IPM had the most variability in flow rates at the outlets (Fig. 7D). At an inlet flow rate of 55 µl min^{-1}, all PDMS devices irrespective of fabrication method had an average positive outlet flow rate ranging from 6.92 to 23.49 µl min^{-1} (Fig. 7E). Once again, the PDMS devices cast from the master molds micromilled at 35 IPM had the highest average outlet flow rate but also had the highest variability between outlet flow rates (Fig. 7E). Lastly, at an inlet flow rate of 100 µl min^{-1}, the average outlet flow rate for all µ-split devices approached the perfect theoretical splitting value (50 µl min^{-1}) with average outlet flow rates ranging from 43.14 to 55.88 µl min^{-1}

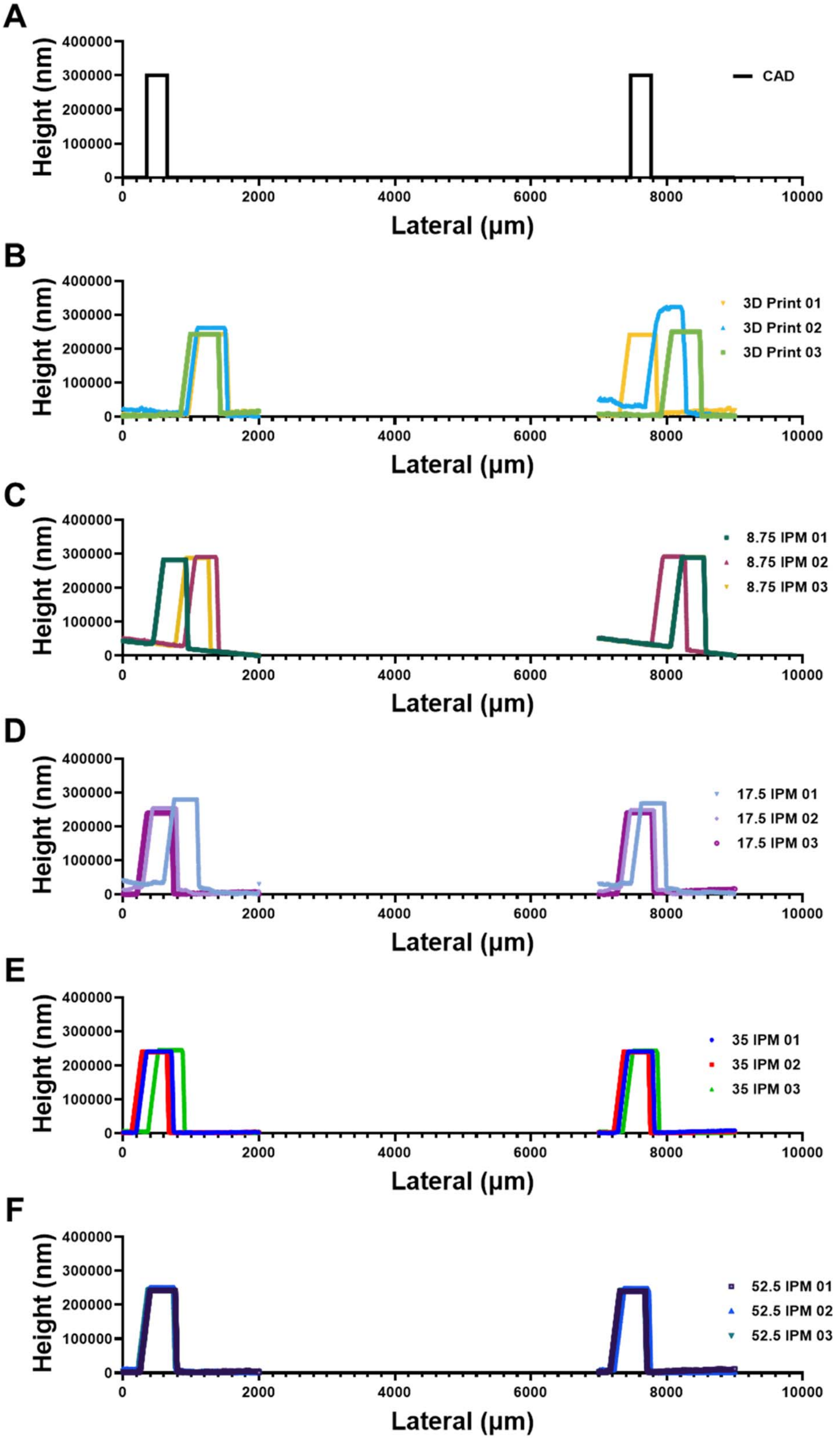

Fig. 5 Outlet profilometer measurements from master molds of microfluidic splitters. (A) Graph of theoretical outlet profilometer measurements of microfluidic splitter master mold retrieved from CAD file. Profilometer measurement from microfluidic splitter outlet master molds fabricated using (B) 3D printing and (C–F) micromilling. Data represents profilometer measurements from $N = 3$ from single master molds per fabrication method.

irrespective of the fabrication method used for the master mold (Fig. 7F). Again, the PDMS device cast from the master molds micromilled at 35 IPM had the highest variability at the outlet flow rates (Fig. 7F).

To better understand the efficacy at which each PDMS μ-split device splits low-flow rates, we proceeded to calculate flow rate splitting efficiency using the ratio of the right outlet and left outlet volumetric measurements. We then created a plot of the flow rate splitting efficiency ratio at each inlet flow rate (5, 19, 35, 55, and 100 μl min^{-1}). In an ideal scenario, the flow rate splitting efficiency ratio should be 1 indicating the device equally splits the flow rate between both outlets. At an inlet flow rate of 5 μl min^{-1}, the average splitting efficiency ratio is very high for all devices (1.7 to 23), indicating inefficient flow rate splitting at the outlet channels (SI Fig. 3). This is mainly due to the stalling and backflow at certain outlets, irrespective of fabrication method of the master mold. The average flow rate splitting efficiency drastically improves, approaching a splitting efficiency ratio of 1 as we near higher flow rates (19, 35, and 55 μl min^{-1}) for most fabrication methods with exception of the PDMS μ-split devices cast from the master molds micromilled at 17.5 IPM (SI Fig. 3). At a flow rate of 100 μl min^{-1}, all PDMS μ-split devices closely approximated a perfect splitting ratio of 1 with the average flow rate splitting efficiency ranging from 0.84 to 1.5, irrespective of the fabrication methods used for creating the master mold (SI Fig. 3). We compared the variance of the average flow rate splitting efficiency ratio at each inlet flow rate using one-way ANOVA and found no statistically significant differences between any of the fabrication methods used for creating the μ-split master molds.

Additionally, we explored the effects of varying the ratio between the curing agent and elastomer utilize to make our PDMS microfluidic chips on our flow rate splitting efficiency. Using the master molds micromilled at 35 IPM, we cast PDMS microfluidic chips with varying ratios of curing agent to elastomer (1 : 5, 1 : 9, and 1 : 20), proceeded to repeat our low-flow splitting assay (5, 19, 35, 55, and 100 μl min^{-1}), and calculated the flow rate splitting efficiency. The results of our experiments revealed that ratio of 1 : 5 (curing agent: elastomer) had a flow rate splitting efficiency comparable to our original ratio of 1 : 9 across all inlet flow rates (SI Fig. 4). The PDMS chips made using a ratio of 1 : 20 performed poorly at evenly splitting flow, this was most evident when the inlets were perfused at 19 and 35 μl min^{-1} resulting in an average of flow rate splitting efficiency of 145.64 and −82.157 respectively. Like our previous comparison between 3D printed and micromilled master molds using varying feed rates, all three varying ratios of curing agent and elastomer (1 : 5, 1 : 9, and 1 : 20) approached an average flow rate splitting efficiency ratio of 1 (0.64–1.498) once the inlet flow rate increased to 100 μl min^{-1} (SI Fig. 4).

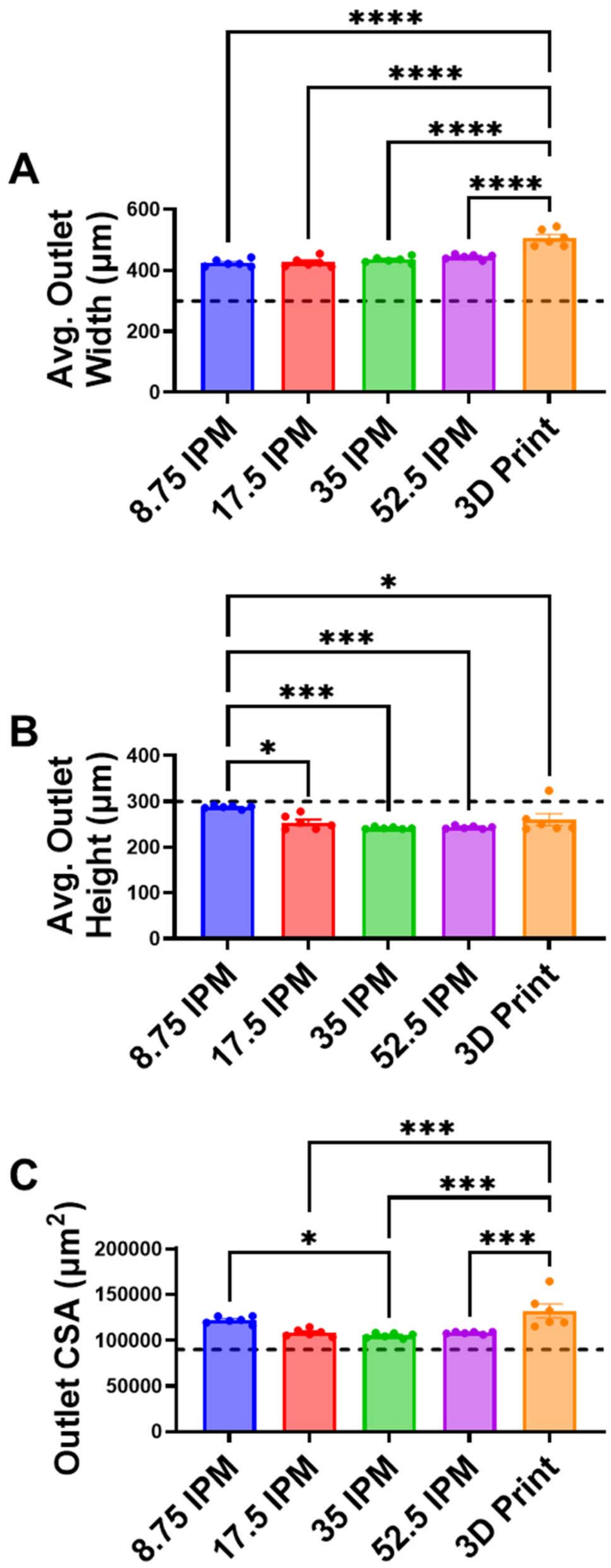

Fig. 6 Quantification of outlet profilometer measurements. Outlet profilometer measurement plots from each master mold were used to measure the average inlet (A) width, (B) height and (C) cross-sectional area (CSA). Data represents mean ± SEM from $N = 6$ from single master mold outlet per fabrication method. Statistical significance was calculated using a one-way ANOVA comparing all the fabrication modalities to each other (8.75 IPM *vs.* 17.5 IPM, 8.75 IPM, *vs.* 35 IPM, 8.75 IPM *vs.* 52.5 IPM, 8.75 IPM *vs.* 3D print, 17.5 IPM *vs.* 35 IPM, 17.5 IPM *vs.* 52.5 IPM, 17.5 IPM *vs.* 3D print, 35 IPM *vs.* 52.5 IPM, 35 IPM *vs.* 3D print, and 52.5 IPM *vs.* 3D print; *, $p < 0.05$; ***$p < 0.001$; ****, $p < 0.0001$). Dotted lines represent the width, height, and cross-sectional area from the CAD model of the μ-split master mold.

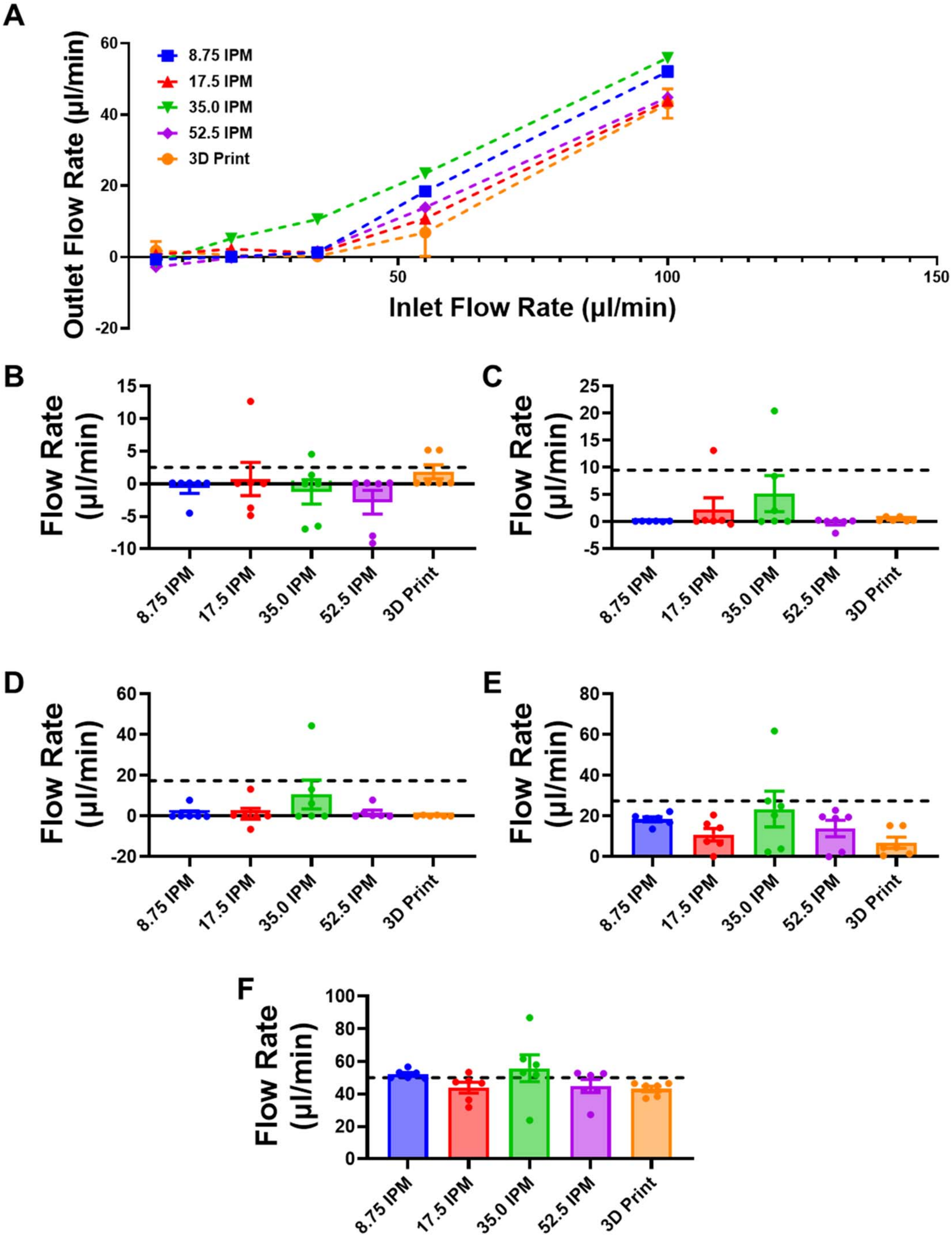

Fig. 7 Flow rate characterization of microfluidic splitters. (A) Line graphs of flow rate measurements from microfluidic splitter outlets. Average flow rate of each microfluidic splitter outlet at various inlet flow rate velocities including (B) 5, (C) 19, (D) 35, (E) 55, and (F) 100 µl min^{-1}. Dotted line in each bar graph represents the expected value for equally splitting the inlet flow rate. Data represents mean ± SEM from $N = 6$ from single master mold outlet per fabrication method. Statistical significance was calculated using a one-way ANOVA applied to each fabrication method (*, $p < 0.05$; ***, $p < 0.001$; ****, $p < 0.0001$).

Effects of microfluidic fabrication tolerances on the production of gelatin microspheres

Lastly, we decided to test a secondary application for evaluating the effects of fabrication tolerances in a flow focusing microfluidic device designed for generating gelatin microspheres (Fig. 8A and B). We fabricated 3 master mold replicates of the flow focusing microfluidic device using 3D printing and micromilling (Fig. 8C). We proceeded to measure the channel dimensions and calculated the cross-sectional area (CSA) of the flow focusing channel and the main channel. We found no statistically significant differences in the CSA of the flow focusing channel (~700 000 µm^2; Fig. 8D) or the main channel

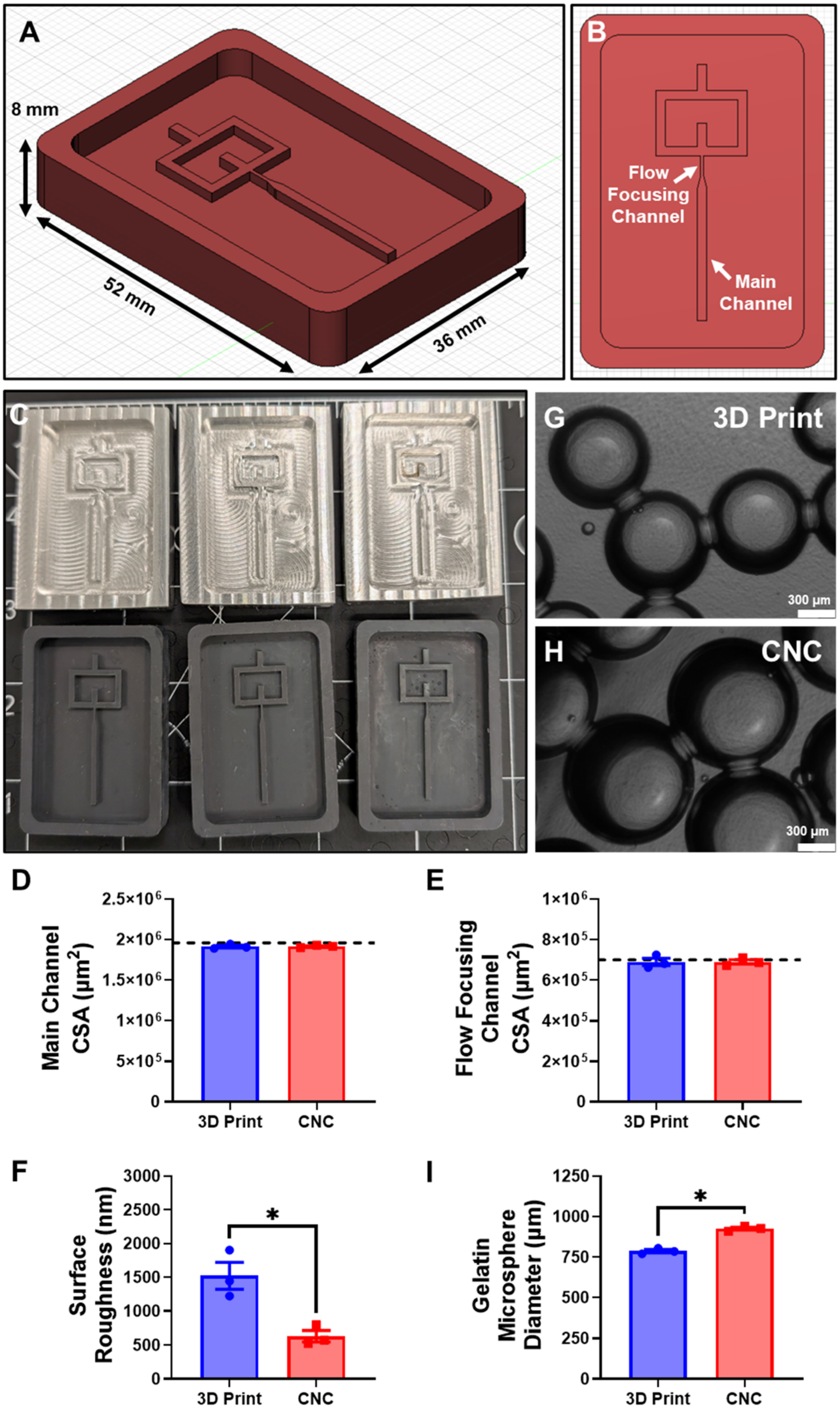

Fig. 8 Comparison of gelatin microspheres generated using a flow focusing microfluidic casted from a 3D printed and micromilled master molds. Diagrams generated using CAD software of (A) angled and (B) top view of flow focusing microfluidic master mold. (C) Pictures of fabricated flow focusing microfluidic master molds using 3D printing and micromilling. Cross sectional area measurements of (D) main channel and (E) flow focusing channel of the fabricated flow focusing microfluidic master molds. (F) Calculated surface roughness from profilometry measurements of 3D printed and micromilled master molds. Pictures of gelatin microspheres generated using microfluidic chips casted from (G) 3D printed and (H) micromilled master molds (scale bar = 300 µm). (I) Diameter measurements of gelatin microspheres generated using flow focusing microfluidic chips. Dotted lines represent the cross-sectional area (CSA) from the CAD model of the flow focusing microfluidic master mold. Data represents mean ± SEM from $N = 3$ from single master mold per fabrication method. Statistical significance was calculated using an unpaired Student's t-test (*, $p < 0.05$).

(~1 960 000 μm^2; Fig. 8E) between the different fabrication modalities. We calculated the surface roughness from our profilometry measurements across the top of the flow focusing channel and main channel. There was a statistically significant difference in the average surface roughness between the 3D printed (1524 nm) and micromilled (632 nm) master molds (Fig. 8F). We proceeded to generate multiple batches of thermally cross-linked gelatin microspheres using flow focusing microfluidic devices cast from the 3D printed or micromilled master molds (Fig. 8G and H). Quantification of the gelatin microspheres showed a statistically significant difference in the average diameter of gelatin microspheres generated between the flow focusing devices from the 3D printed (787 μm) and micromilled (926 μm) master molds (Fig. 8I).

Conclusions

This investigation is intended to function as a guide for future researchers creating microfluidic master molds using 3D printing and micromilling. For micromilling, our profilometry measurements indicate that the only significant difference was for the master molds at 8.75 IPM. We hypothesize that the major differences in the channels heights were primarily due to the use of a new 0.125″ flat end mill as the previous 0.125″ end mill use for micromilling the rest of the master molds (17.5, 25, and 52.5 IPM) broke when we attempted to fabricate master molds using a feed rate of 140 IPM. Thus, the difference in the channel heights for the master molds micromilled at 8.75 IPM is a function of the tolerances of the flat end mills (~75 μm) used during the micromilling process. Overall, irrespective of the fabrication method (3D printing or micromilling), the fabricated channels tended to be shorter and narrower when compared to the CAD model. We also noted a difference on the surface finish of the master molds that were 3D printed *versus* the ones that were micromilled. Micromilled master molds had a smoother finish with the average surface roughness of ~300 nm while the 3D printed master molds had an average surface roughness of ~1700 nm, an entire order of magnitude higher. In our low-flow rate splitting experiments, we did not notice any significant differences in performance between devices made from different master molds. This is especially interesting as our average surface roughness were statistically significantly different between the 3D printed and the micromilled master molds. Low-flow rate splitting remains a challenging endeavor due to the dominance of surface tension and hydrodynamic resistance that is amplified in microfluidic devices. We hypothesize that surface tension and hydrodynamic resistance play a dominant role in the flow rate splitting efficiency more so than average surface roughness. This was the most apparent at an inlet flow rate of 5 μl min^{-1} where the majority of the PDMS μ-split devices had either stalled flow or back flow at one of the outlet channels. The average flow rate splitting efficiency only normalized when we increased the inlet flow rate. This was the most evident in our highest inlet flow rate condition (100 μl min^{-1}). Interestingly, the PDMS μ-split devices from the master molds micromilled at 17.5 IPM had the worst splitting efficiency ratio, it is unclear why this occurred. To conclude our testing on the effects of microfluidic fabrication tolerances on low-flow rate splitting, we proceeded to test different ratios of PDMS curing agent and elastomer (1 : 5, 1 : 9, and 1 : 20). Interestingly, we noticed more variability in the flow rate splitting efficiency in the PDMS μ-split devices made using a 1 : 20 ratio of curing agent and elastomer. Like our previous testing, increasing the flow rate made all μ-split devices, irrespective of curing agent and elastomer ratio combination (1 : 5, 1 : 9, and 1 : 20), approach a flow rate splitting efficiency of 1, indicating even splitting between both outlets of the μ-split devices. We hypothesize that other factors such as tooling tolerances, master mold cleanliness, and PDMS microfluidic device assembly may also play a role that significantly alters the performance of microfluidic devices in low-flow rate splitting applications. Although micromilling results in smoother surface finish, our data demonstrates no significant differences between PDMS μ-split devices cast from either micromilled or 3D printed master molds in our low-flow rate splitting application.

In our second application utilizing a flow focusing microfluidic device to generate gelatin microspheres we did not notice any significant differences in the channel dimensions between flow focusing microfluidic device cast from 3D printed or micromilled master molds. Similarly to our μ-split devices, we noticed that there was a significant difference in average surface roughness between 3D printed and micromilled master molds, with CNC molds being 3 times smoother than the 3D printed master molds. In this application the difference in average surface roughness led to the generation of different size gelatin microspheres. The flow focusing microfluidic chips cast from the CNC master molds generated gelatin microspheres that were approximately 140 μm larger in diameter. We hypothesize that the smoother surface finish in the flow focusing microfluidic device cast from the micromilled master molds reduces the shear stress along the walls of the PDMS device, creating a thinner oil film along the walls, and reducing turbulent flow. This in turn allows for the gelatin microspheres to grow before being pinched off at the flow focusing channel segment, resulting in a larger average diameter microsphere even though we utilized the same flow rates during our experimentation. The results of this second application highlight the importance of fabrication tolerances and their impact on experimental outcomes. We would like to highlight to our reader that tighter fabrication tolerances can be achieved by using different fabrication procedures such as those performed in a cleanroom using SU-8 photolithography which can result on average surface roughness ranging from 1 nm[14] to 10 nm.[15] When fabricating a microfluidic chip, we would like our readers to carefully consider whether your microfluidic application will be sensitive to the fabrication tolerances achieved by your fabrication method of choice (3D printing, micromilling, of SU-8 photolithography). Thorough testing must be performed when switching fabrication modalities to ensure that fabrication tolerances are not altering your microfluidic application outcomes.

The major advantages of 3D printed master molds are their ability to rapidly fabricate prototypes, cheaper fabrication cost, and user friendliness. Additionally, 3D printing allows for the creation of more intricate 3D designs that micromilling might not be able to create due to constraints with tooling operations and dimensions. The tradeoff for these advantages is the brittleness of 3D printed master mold which can lead to cracking or breakage as well as its limited lifetime. In our experience, 3D printed microfluidic master molds last approximately 10 to 15 cast cycle before signs of wear and tear appear. This makes 3D printed master molds ideal for rapidly iterating prototype designs in the laboratory or for microfluidic designs that would be impossible to fabricate using micromilling. In contrast, micromilled aluminum master molds offer a longer lifetime (if properly cleaned and maintained) which can last hundreds if not thousands of cast cycles before signs of wear and tear appear. This make micromilled aluminum master highly desirable for the mass production of a finalized microfluidic design such as for commercial production. However, creating micromilled aluminum master molds is more expensive than their 3D printed counterparts and requires more training to successfully mill an aluminum master mold. We hope our work acts as an initial guide for future researchers in their fabrication endeavors to produce 3D printed and micromilled master molds.

Author contributions

DC was responsible for the conceptualization of the project. AKY designed the microfluidic splitter device. Formal analysis of data, methodology, data visualization, software, and validation were completed by DC, IO, and MLR. Primary investigation was performed by DC, IO, and MLR. Funding acquisition and supervision was provided by ESL. Writing of the original draft was performed by DC. All authors participated in the reviewing and editing process of the manuscript draft.

Conflicts of interest

The authors declare that the research was conducted in the absence of any commercial or financial relationships that could be construed as a potential conflict of interest.

Data availability

All data files including raw profilometry measurements, volumetric measurements, CNC toolpaths, CAD files, and Graphpad files from this work are available at: https://github.com/DrChavarria/Microfluidic-Splitter.

Supplementary information (SI) is available. See DOI: https://doi.org/10.1039/d6ra00916f.

Acknowledgements

The author(s) declared that financial support was received for the research, authorship, and/or publication of this article. Funding for this work was provided by a Chan Zuckerberg Initiative Ben Barres Early Career Acceleration Award 2019-191850 (to ESL), NIH grant R01 NS110665 (to ESL), and NSF grant 1846860 (to ESL). Funding for DC was provided by Vanderbilt Integrated Training in Engineering and Diabetes (T32 DK101003). Funding for IO was provided by the School for Science and Math at Vanderbilt in partnership with Metro Nashville Public Schools. Funding for AKY was provided by the Vanderbilt Interdisciplinary Training Program in Alzheimer's Disease (T32 AG058524). All statistical analysis and graphs completed with GraphPad Prism version 10.6.1 for Windows 11, GraphPad Software, Boston, Massachusetts, USA, https://www.graphpad.com/. Computer aided design (CAD) files were drawn with Autodesk Fusion360 (Windows 11 Home 25H2 [26200.7309]) using an educational license. Stylus profilometers measurements were conducted at the Vanderbilt Institute of Nanoscale Science and Engineering (VINSE).

References

1 E. S. Koselar and R. R. Reston, *Surf. Coat. Technol.*, 1994, **68–69**, 679–685.
2 Y. Xia and G. M. Whitesides, *Angew. Chem., Int. Ed.*, 1998, **37**, 550–575.
3 J. C. Brooks, K. I. Ford, D. H. Holder, M. D. Holtan and C. J. Easley, *Analyst*, 2016, **141**, 5714–5721.
4 B. J. O'Grady, M. D. Geuy, H. Kim, K. M. Balotin, E. R. Allchin, D. C. Florian, N. N. Bute, T. E. Scott, G. B. Lowen, C. M. Fricker, M. L. Fitzgerald, S. A. Guelcher, J. P. Wikswo, L. M. Bellan and E. S. Lippmann, *Lab Chip*, 2021, **21**, 4814–4822.
5 N. Mohd Fuad, M. Carve, J. Kaslin and D. Wlodkowic, *Micromachines*, 2018, **9**, 116.
6 D. J. Guckenberger, T. E. de Groot, A. M. D. Wan, D. J. Beebe and E. W. K. Young, *Lab Chip*, 2015, **15**, 2364–2378.
7 A. Lashkaripour, R. Silva and D. Densmore, *Microfluid. Nanofluidics*, 2018, **22**, 31.
8 C. E. Owens and A. John Hart, *Lab Chip*, 2018, **18**, 890–901.
9 A. Javidanbardan, A. M. Azevedo, V. Chu and J. P. Conde, *Micromachines*, 2021, **13**, 6.
10 M. Tang, X. Cheng, G. Zheng, H. Liu, X. Li and J. Liu, *Ceram. Int.*, 2024, **50**, 11167–11178.
11 A. K. Yates, H. N. Murray and E. S. Lippmann, *SLAS Technol.*, 2025, **32**, 100305.
12 D. Chavarria, K. A. Georges, B. J. O'Grady, K. K. Hassan and E. S. Lippmann, *Front. Bioeng. Biotechnol.*, 2025, **13**, 1494553.
13 A. I. Romero-Morales, B. J. O'Grady, K. M. Balotin, L. M. Bellan, E. S. Lippmann and V. Gama, *HardwareX*, 2019, **6**, e00084.
14 S. Anbumani, A. M. da Silva, A. Alaferdov, M. V. Puydinger dos Santos, I. G. B. Carvalho, M. de Souza e Silva, S. Moshkalev, H. F. Carvalho, A. A. de Souza and M. A. Cotta, *ACS Appl. Bio Mater.*, 2022, **5**, 4903–4912.
15 K. D. Vora, B. Lochel, E. C. Harvey, J. P. Hayes and A. G. Peele, *J. Manuf. Syst.*, 2006, **16**, 1975.